Microfluid Nanofluid
DOI 10.1007/s10404-013-1280-z

RESEARCH PAPER

Three-dimensional and analytical modeling of microfluidic particle transport in magnetic fluids

Rui Cheng · Taotao Zhu · Leidong Mao

Received: 18 June 2013 / Accepted: 14 October 2013

Abstract We present an analytical model that can predict the three-dimensional (3D) transport of non-magnetic particles in magnetic fluids inside a microfluidic channel coupled with permanent magnets. The magnets produce a spatially non-uniform magnetic field that gives rise to a magnetic buoyancy force on the particles. Resulting 3D trajectories of the particles are obtained by (1) calculating the 3D magnetic buoyancy force exerted on the particles via an analytical distribution of magnetic fields as well as their gradients, together with a nonlinear magnetization model of the magnetic fluids, (2) deriving the 3D hydrodynamic viscous drag force on the particles with an analytical velocity profile of a low Reynolds number ferrohydrodynamic flow in the channel including "wall effect" and magnetoviscous effect of the magnetic fluids, and (3) constituting and solving the governing equations of motion for the particles using the analytical expressions of magnetic buoyancy force and hydrodynamic viscous drag force. We use such a model to study the particles' trajectories in the channel and investigate the magnitude of their deflections at different flow rates, with different properties of magnetic fluids and different geometrical parameters of the system.

Keywords Microfluidics · Particle transport · Magnetic fluids · Ferrofluids · Three-dimensional · Particle separation

R. Cheng · L. Mao (✉)
College of Engineering, Nanoscale Science and Engineering Center, University of Georgia, Athens, GA 30602, USA
e-mail: mao@uga.edu

T. Zhu
Department of Chemistry, Nanoscale Science and Engineering Center, University of Georgia, Athens, GA 30602, USA

1 Introduction

Microfluidic particle transport has generated a lot of enthusiasm in the past decade for its potential applications in diagnostics (Nagrath et al. 2007; Adams et al. 2008; Hoshino et al. 2011; Mao and Huang 2012b), therapeutics (Toner and Irimia 2005; Yung et al. 2009) and environmental monitoring (Liu et al. 2004; Beyor et al. 2008; Dharmasiri et al. 2010). Techniques developed to transport particles and cells so far were mainly based on their intrinsic physical properties for manipulation specificity (Pamme 2007; Tsutsui and Ho 2009; Gossett et al. 2010; Lenshof and Laurell 2010; Robert et al. 2011; Mao and Huang 2012a; Tarn et al. 2013). Thanks to their high throughput, low-cost and lacking of labeling steps in most cases, these techniques were often preferred over existing label-based macro-scale techniques such as fluorescence-activated sorter (FACS) (Bonner et al. 1972). Among them, those based on passive microchannel geometry including pinched flow fractionation (Yamada et al. 2004) and deterministic lateral displacement (Huang et al. 2004; Davis et al. 2006) combined laminar flows with microchannel structures to direct particles of different sizes or deformability (McFaul et al. 2012) into separate streamlines. At the same time, external energy inputs including acoustic, electric and magnetic forces have also been used for manipulations. For instances, acoustophoresis was used to separate particles and cells according to their size, density, as well as compressibility (Laurell et al. 2007; Shi et al. 2009; Wang and Zhe 2011). Dielectrophoresis (DEP) realized low-cost and integrated devices for cell manipulation (Voldman 2006; Pethig 2010). Magnetophoresis was applied to separate paramagnetic red blood cells or bacteria from other species (Zborowski et al. 2003; Lee et al. 2004). Magnetophoresis is a label-based technique (Pamme 2006;

Published online: 27 October 2013

Liu et al. 2009; Gijs et al. 2010), which could be manually intensive and time-consuming when compared to label-free techniques. Recently, non-magnetic particles, cells and droplets manipulation in magnetic fluids have been investigated for its unique advantage as a label-free technique (Kose et al. 2009; Zhu et al. 2011a; Shen et al. 2012). It is often referred as "negative magnetophoresis". Non-magnetic objects within magnetic fluids, experiencing a volume-dependent magnetic buoyancy force under a non-uniform magnetic field, can be manipulated toward the weaker field direction, enabling many different microfluidic applications including particles assembly (Yellen et al. 2005; He et al. 2010), particles trapping (Winkleman et al. 2004; Zhang et al. 2011), particles focusing (Zhu et al. 2011a; Zeng et al. 2012), particles and cells separation (Kose et al. 2009; Shen et al. 2012; Vojtíšek et al. 2012; Zhu et al. 2012).

Commonly used magnetic fluids for microfluidic manipulations include both paramagnetic salt solutions and ferrofluids. Aqueous solutions of paramagnetic salts of elements, such as manganese and gadolinium having unfilled inner subshells with unpaired electrons, provide low-susceptibility and high-saturation magnetic fluids. For instance, the typical susceptibility of $MnCl_2$ is on the order of 10^{-4}, and its saturation magnetization at 20 Tesla can reach 10^4 A/m at a solubility limit of 1,470 kg/m^3 (Rosensweig 1985). Ferrofluids, on the other hand, are colloidal suspensions of magnetic nanoparticles (Rosensweig 1985). These nanoparticles, normally magnetite (Fe_3O_4) with approximate 10 nm diameter, are covered by either electrostatic or steric surfactants to keep them apart and suspended within a compatible carrier medium. Concentrations of nanoparticles can be adjusted in ferrofluids with a maximum volume fraction up to 10 %. Susceptibility of ferrofluids can reach as high as 1, approximately 4–5 orders larger than a typical paramagnetic salt solution. Saturation magnetization of ferrofluids depends on its material type and volume fraction of magnetic materials. A magnetite-based ferrofluid with 1 % volume fraction has a saturation magnetization of 4.46×10^3 A/m. Compared to paramagnetic salt solutions, ferrofluids have both higher initial magnetic susceptibility and higher magnetization at practical magnetic fields from a permanent magnet (less than 1 Tesla). These attributes of ferrofluids could lead to fast manipulation of non-magnetic objects in them, rendering high throughput in separation devices (Zhu et al. 2010, 2012).

Magnetic fields can be produced by either a permanent magnet or a microfabricated electromagnet. The features and capabilities of different magnetic field sources in microsystems have been well documented (Liu et al. 2009; Gijs et al. 2010). Compared to microfabricated electromagnets, permanent magnets generally have large magnetic fields but smaller field gradients. On the other hand, permanent magnet-based devices do not need expensive microfabrication process or auxiliary power supply. They are easy to operate and do not generate heat during operation. These advantages may overweigh its drawback in applications where low-cost and simple operation is preferred.

Fast optimization of these permanent magnet-based microfluidic devices is critical to their applications. It has been experimentally demonstrated that particles' transport in ferrofluids was directly affected by the magnetic buoyancy force and hydrodynamic viscous drag force, both of which were dependent on parameters such as fluid properties and device geometries (Zhu et al. 2010, 2011a, b, 2012). For instance, they include ferrofluids flow rate, concentration of ferrofluids, microchannel geometry and magnet dimension. Systematic optimization of these parameters via experimental methods takes too much time and resources. Therefore, analytical models of particles' transport are often favored to enable accurate and fast parametric optimization of microfluidic system before device fabrication. A two-dimensional (2D) analytical model of magnetophoresis has been developed for such purpose (Furlani 2006, 2007; Furlani and Sahoo 2006). Similarly, a 2D "negative magnetophoresis" model was later developed to investigate the transport of non-magnetic particles in magnetic fluids and its validity has been confirmed by experimental results (Zhu et al. 2011b). Here, we present a three-dimensional (3D) analytical model of microfluidic particle transport in magnetic fluids. The 2D model developed before only considers particle transport in the plane that is perpendicular to the channel depth, and assume the particle is fixed at a specific position along the channel depth. This assumption is not valid in most of realistic experimental setups, where particles are free to flow along the channel depth, on which its velocity closely depends. Our new model on the other hand provides comprehensive information of particles' trajectory in 3D and is much closer to real experimental conditions. It takes into account important optimization parameters including fluid properties, magnet dimensions and relative positions of the magnet to the channel, and provides crucial information such as magnetic fields distribution, forces, particle velocity and trajectory in 3D. We envision this model can be used to perform quick and accurate 3D parametric optimizations for magnetic fluid-based microfluidic devices. The 3D model developed here is not limited to permanent magnet-based devices; it can also be applied toward electromagnet-based microfluidic systems provided that the expressions of magnetic field distribution are known.

In the following sections, we start by obtaining the magnetic field distribution through an analytical formula, and then introduce the dominant forces in our model, followed by a discussion on magnetoviscous effect of magnetic fluids. A coupled ordinary differential equation (ODE) system consisted of equations of particles motion in 3D is solved numerically to obtain particles transport in a rectangular microchannel coupled with permanent magnets. Dependence of particles' transport on fluid properties and microchannel/magnet dimensions are summarized and discussed.

2 Theory

A non-magnetic object of micrometer size in a microchannel filled with magnetic fluids experiences several types of forces under the influence of a permanent magnet (Furlani 2006). It has been shown that the magnetic buoyancy force and hydrodynamic viscous drag force were the dominant forces when compared to gravitational, buoyant, diffusive and *Derjaguin-Landau-Verwey-Overbeek* (DLVO) forces (Zhu et al. 2011b). DLVO force is a combination of the van der Waal's force and the electrostatic force between particles and surfaces. Both forces can be rendered repulsive after proper chemical treatment of the channel to avoid undesirable surface problems such as particles sticking to the channel surface (Liu et al. 2009). DLVO force can then be neglected. Therefore, we will focus our discussion on these two forces that start with an analysis of magnetic fields.

2.1 Magnetic field analysis

An analytical expression was used to simulate 3D magnetic field strength distribution $\vec{H}(x,y,z)$ produced by a rectangular permanent magnet (Furlani 2001). As shown in Fig. 1, a rectangular magnet is placed at the origin of the Cartesian coordinates.

Because of the symmetric configuration of the magnet, x component and z component of the magnetic field strength, H_x and H_z, have similar expressions as

$$H_x = \frac{M_s}{4\pi}\sum_{k=1}^{2}\sum_{m=1}^{2}(-1)^{k+m} \times \ln\left\{\frac{(z-z_1)+\left[(x-x_m)^2+(z-z_1)^2+(y-y_k)^2\right]^{1/2}}{(z-z_2)+\left[(x-x_m)^2+(z-z_2)^2+(y-y_k)^2\right]^{1/2}}\right\} \quad (1)$$

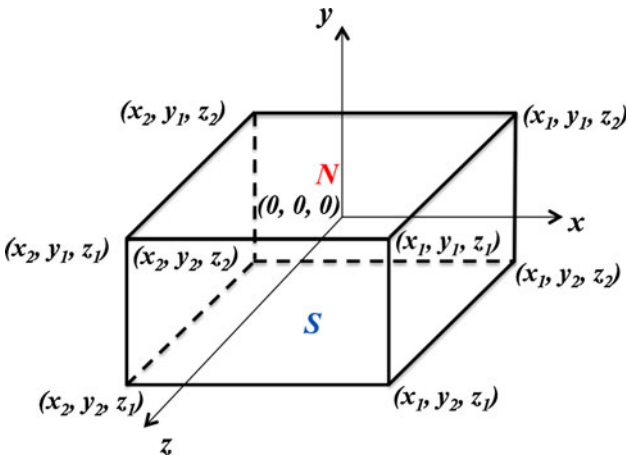

Fig. 1 A rectangular permanent magnet located in Cartesian coordinates with its magnetization facing negative y-direction. *Eight corners* of the magnet are at (x_1, y_1, z_1), (x_1, y_1, z_2), (x_1, y_2, z_1), (x_1, y_2, z_2), (x_2, y_1, z_1), (x_2, y_1, z_2), (x_2, y_2, z_1) and (x_2, y_2, z_2)

$$H_z = \frac{M_s}{4\pi}\sum_{k=1}^{2}\sum_{m=1}^{2}(-1)^{k+m} \times \ln\left\{\frac{(x-x_1)+\left[(x-x_1)^2+(z-z_m)^2+(y-y_k)^2\right]^{1/2}}{(x-x_2)+\left[(x-x_2)^2+(z-z_m)^2+(y-y_k)^2\right]^{1/2}}\right\} \quad (2)$$

Parallel to the direction of polarization, y component of magnetic field strength H_y is

$$H_y = \frac{M_s}{4\pi}\sum_{k=1}^{2}\sum_{n=1}^{2}\sum_{m=1}^{2}(-1)^{k+n+m} \times \tan^{-1}\left\{\frac{(x-x_n)(z-z_m)}{(y-y_k)\left[(x-x_n)^2+(z-z_m)^2+(y-y_k)^2\right]^{1/2}}\right\} \quad (3)$$

Here, M_s is magnetization of the permanent magnet. Magnetic fields produced by a rectangular magnet can be fully represented by Eqs. (1), (2) and (3) in 3D. From the expressions of magnetic field strength, we obtained field gradients in an analytical manner using a mathematical tool Maple Version 14 (Waterloo Maple Inc. Waterloo, Ontario, Canada). The expressions of field gradients are too long to list here.

2.2 Magnetic buoyancy force

Non-magnetic objects inside magnetic fluids under a non-uniform magnetic field experience a magnetic buoyancy force $\vec{F}_m$, which can be derived from a Maxwell stress tensor (Rosensweig 1985).

$$\vec{F}_m = \oiint \left(\frac{1}{2}\mu_0 M_n^2 + \mu_0 \int_0^H M \mathrm{d}H \right) \vec{n} \mathrm{d}S \tag{4}$$

Equation (4) presents the magnetic buoyancy force in its integral form, in which S is the surface just enclosing a non-magnetic object in magnetic fluids, $\vec{n}$ is a unit vector with its direction pointing normally outwards the surface, H is the magnitude of magnetic field strength, and M is the magnitude of magnetization of magnetic fluids with its normal component M_n in regard to the enclosing surface. With dilute magnetic fluids and intense magnetic fields, $\frac{1}{2}M_n^2/\bar{M}H \ll 1$, where $\bar{M}$ is field-averaged magnetization of magnetic fluids. Therefore, magnetic buoyancy force on a non-magnetic object inside magnetic fluids can be simplified to

$$\vec{F}_m = -\mu_0 V (\vec{M} \cdot \nabla)\vec{H} \tag{5}$$

Here, V is volume of the non-magnetic object immersed in the magnetic fluid, $\vec{M}$ is the vector of magnetization, and $\vec{H}$ is the vector of magnetic field strength at the center of the particle. The presence of a minus sign in front of the expression indicates that the magnetic buoyancy force is pointing in the direction of the weaker magnetic field.

Under the condition of non-interacting magnetic nanoparticles in dilute ferrofluids, the magnetic fluid is magnetized by external fields following a Langevin function (Rosensweig 1985) that can be described as

$$\frac{M(H)}{\phi M_d} = L(\kappa) = \coth(\kappa) - \frac{1}{\kappa}$$

where

$$\kappa = \frac{\mu_0 \pi M_d d^3 H}{6 k_B T} \tag{6}$$

Here, M_d is bulk magnetization of magnetic nanoparticles of diameter d, which are suspended in a carrier medium with volume fraction ϕ. k_B is the Boltzmann constant, and T is the temperature.

Expanding Eq. (5) in 3D, we obtain the expression of magnetic buoyancy force as

$$\vec{F}_m = -\mu_0 V \begin{pmatrix} M_x \frac{\partial H_x}{\partial x} + M_y \frac{\partial H_x}{\partial y} + M_z \frac{\partial H_x}{\partial z} \\ M_x \frac{\partial H_y}{\partial x} + M_y \frac{\partial H_y}{\partial y} + M_z \frac{\partial H_y}{\partial z} \\ M_x \frac{\partial H_z}{\partial x} + M_y \frac{\partial H_z}{\partial y} + M_z \frac{\partial H_z}{\partial z} \end{pmatrix} \tag{7}$$

For systems with more than one permanent magnet ($n > 1$, n is the number of magnets), magnetic fields can be superimposed and the magnetic buoyancy force takes the expression of

$$F_m = -\mu_0 V \begin{pmatrix} M_{x(\sum_{i=1}^n H_x^i)} \frac{\partial(\sum_{i=1}^n H_x^i)}{\partial x} + M_{y(\sum_{i=1}^n H_y^i)} \frac{\partial(\sum_{i=1}^n H_x^i)}{\partial y} + M_{z(\sum_{i=1}^n H_z^i)} \frac{\partial(\sum_{i=1}^n H_x^i)}{\partial z} \\ M_{x(\sum_{i=1}^n H_x^i)} \frac{\partial(\sum_{i=1}^n H_y^i)}{\partial x} + M_{y(\sum_{i=1}^n H_y^i)} \frac{\partial(\sum_{i=1}^n H_y^i)}{\partial y} + M_{z(\sum_{i=1}^n H_z^i)} \frac{\partial(\sum_{i=1}^n H_y^i)}{\partial z} \\ M_{x(\sum_{i=1}^n H_x^i)} \frac{\partial(\sum_{i=1}^n H_z^i)}{\partial x} + M_{y(\sum_{i=1}^n H_y^i)} \frac{\partial(\sum_{i=1}^n H_z^i)}{\partial y} + M_{z(\sum_{i=1}^n H_z^i)} \frac{\partial(\sum_{i=1}^n H_z^i)}{\partial z} \end{pmatrix} \tag{8}$$

2.3 Hydrodynamic viscous drag force

Reynolds number in a typical microfluidic system is very small and much less than 1. As a result, microfluidic flow is laminar and the hydrodynamic viscous drag force exerting on an object is produced by the relative motion between the particle and its surrounding fluid flow. Its expression takes the form of

$$\vec{F}_d = -3\pi\eta D_p (\vec{U}_p - \vec{U}_f) f_D \tag{9}$$

Here, η is viscosity of magnetic fluids, D_p is diameter of a spherical particle, $\vec{U}_p$ and $\vec{U}_f$ are velocity vectors of magnetic fluids and the particle, respectively, f_D is hydrodynamic drag force coefficient of a moving particle considering the influence with a solid surface in its vicinity, which is referred to as the "wall effect." It is a resistance function of hydrodynamic interaction between the particle and the surface. Its appearance indicates the particle experiences increased fluid viscosity as it moves closer to the microchannel surface (Ganatos et al. 1980; Krishnan et al. 1995; Staben et al. 2003),

$$f_D = \left[1 - \frac{9}{16}\left(\frac{D_p}{D_p + 2\Delta}\right) + \frac{1}{8}\left(\frac{D_p}{D_p + 2\Delta}\right)^3 - \frac{45}{256}\left(\frac{D_p}{D_p + 2\Delta}\right)^4 - \frac{1}{16}\left(\frac{D_p}{D_p + 2\Delta}\right)^5 \right]^{-1} \tag{10}$$

Here, Δ is the shortest distance between the channel wall and the surface of the particle.

In order to evaluate the hydrodynamic drag force in Eq. (9), the velocity profile of a fully developed laminar flow in a rectangular microchannel of width w_c and height h_c can be analytically described as (Brody et al. 1996; Ichikawa et al. 2004)

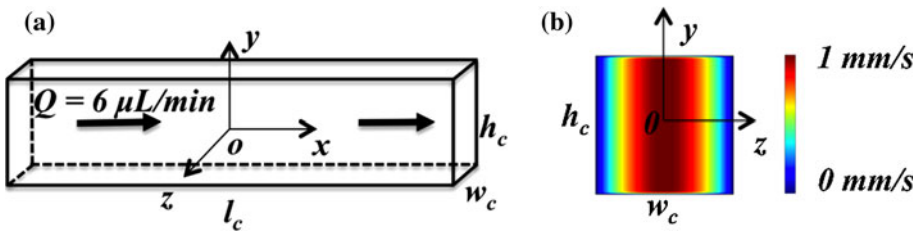

Fig. 2 **a** Dimensions of a microchannel (listed in Table 1) with length l_c, height h_c and width w_c. A laminar flow with flow rate 6 μL/min is introduced into the channel in positive x-direction. **b** A representative velocity distribution in the y–z plane at flow rate 6 μL/min

$$U_f(y,z) = \frac{\pi Q}{2w_c h_c}\left(\frac{a}{b}\right)$$

where

$$a = \sum_{n=0}^{\infty} \frac{(-1)^n \cos\left[\frac{(2n+1)\pi z}{w_c}\right]}{(2n+1)^3}\left[1 - \frac{\cosh\left[\frac{(2n+1)\pi y}{w_c}\right]}{\cosh\left[\frac{(2n+1)\pi h_c}{2w_c}\right]}\right]$$

$$b = \sum_{n=0}^{\infty} \frac{1}{(2n+1)^4}\left[1 - \frac{tanh\left[\frac{(2n+1)\pi h_c}{2w_c}\right]}{\frac{(2n+1)\pi h_c}{2w_c}}\right] \quad (11)$$

Here, Q is the flow rate and the channel is set in Cartesian coordinates shown in Fig. 2a. The smallest dimension of the microchannel used in our simulation is on the order of 10 μm, much larger the diameter of the fluidic channel in which "slip" boundary condition becomes evident (Huang et al. 2006; Wang and Zhao 2011). Therefore, we choose to use "non-slip" boundary conditions when obtaining the velocity profile in the microchannel. Figure 2b depicts a representative flow profile in the cross-section y–z plane.

2.4 Magnetoviscous effect of ferrofluids

The phenomenon of field-dependent changes in viscosity of a suspension of magnetic nanoparticles is known as magnetoviscous effect (Odenbach 2002). Viscosity of ferrofluids without magnetic fields depends on two parameters: average diameter d and total volume fraction ϕ of magnetic nanoparticles (Rosensweig 1985; Odenbach 2002). These two parameters can be used in a model to predict viscosity of magnetic nanoparticles as simple mixture of solids and liquids (Odenbach 2002)

$$\eta = \eta_c\left[1 - \frac{5}{2}\left(\frac{d+2\varepsilon}{d}\right)^3\phi + \left(\frac{5}{2}\phi_c - 1\right)\left(\frac{d+2\varepsilon}{d}\right)^6\left(\frac{\phi}{\phi_c}\right)^2\right]^{-1} \quad (12)$$

Here, η and η_c are the viscosities of a ferrofluid and its carrier liquid, respectively, d is the average diameter of magnetic nanoparticles, and ε is the thickness of surfactant layer on the surface of a nanoparticle; ϕ is the volume fraction of magnetic nanoparticles, and ϕ_c is an empirical value of 0.74 for ferrofluids (Rosensweig 1985; Odenbach 2002).

When ferrofluids are placed under strong magnetic fields, magnetic nanoparticles in them tend to form rigid chains aligning to the field direction, which leads to a larger velocity field gradient surrounding the particles and an increase in the overall fluid viscosity. Rosensweig (1985) obtained the following expression to relate viscosity changes to a magnetic field

$$\frac{\Delta\eta}{\eta} = \frac{3}{2}\phi\frac{0.5\kappa L(\kappa)}{1 + 0.5\kappa L(\kappa)}(\sin\theta)^2 \quad (13)$$

Here, $\Delta\eta$ is the increase in viscosity due to the presence of the magnetic field, $L(\kappa)$ and κ is the Langevin function and its parameter defined in Eq. (6), θ is the angle between the flow vortex and the local magnetic field. According to Eq. (13), the maximum percentage of the viscosity increase $\Delta\eta$ is

$$\left(\frac{\Delta\eta}{\eta}\right)_{\max} = \frac{3}{2}\phi \quad (14)$$

Based on the Eq. (14), the increase in ferrofluids viscosity caused by the presence of a magnetic field is only a few percent for dilute ferrofluids. Magnetoviscous effect is typically more pronounced in ferrofluids with higher concentration ($\sim$10 %) where particle–particle interaction starts to dominate (Odenbach 2002). Practical ferrofluids used for microfluidic particles manipulation are mostly water-based with volume faction on the order of 1 %. Therefore, we chose to ignore magnetoviscous effect in our model for simplicity.

2.5 Governing equations of particle motion

Because of the low Reynolds number in a microchannel, inertial effects on the particle are negligible and the motion of a non-magnetic particle in ferrofluid is determined by the balance of hydrodynamic viscous drag force and magnetic buoyancy force.

$$\vec{F}_m + \vec{F}_d = 0 \quad (15)$$

Rewrite the particle velocity $\vec{U}_p$ as the time derivate of its position, we have

Equation (16) is a coupled ordinary differential equation

(ODE) system for the particle trajectory in 3D. We use a fourth-order Runge–Kutta time integration scheme to solve this ODE system.

3D model reduces to a 2D one because of symmetry. Figure 3a depicts the configuration of the magnets used in this simulation. Figure 3b–f shows the magnetic field and

$$\begin{bmatrix} \frac{dx}{dt} \\ \frac{dy}{dt} \\ \frac{dz}{dt} \end{bmatrix} = \begin{bmatrix} U_f(y,z) \\ 0 \\ 0 \end{bmatrix} - \frac{\mu_0 D^2}{18\eta f_D} \begin{pmatrix} M_x\left(\sum_{i=1}^{n} H_x^i\right)\frac{\partial\left(\sum_{i=1}^{n} H_x^i\right)}{\partial x} + M_y\left(\sum_{i=1}^{n} H_y^i\right)\frac{\partial\left(\sum_{i=1}^{n} H_x^i\right)}{\partial y} + M_z\left(\sum_{i=1}^{n} H_z^i\right)\frac{\partial\left(\sum_{i=1}^{n} H_x^i\right)}{\partial z} \\ M_x\left(\sum_{i=1}^{n} H_x^i\right)\frac{\partial\left(\sum_{i=1}^{n} H_y^i\right)}{\partial x} + M_y\left(\sum_{i=1}^{n} H_y^i\right)\frac{\partial\left(\sum_{i=1}^{n} H_y^i\right)}{\partial y} + M_z\left(\sum_{i=1}^{n} H_z^i\right)\frac{\partial\left(\sum_{i=1}^{n} H_y^i\right)}{\partial z} \\ M_x\left(\sum_{i=1}^{n} H_x^i\right)\frac{\partial\left(\sum_{i=1}^{n} H_z^i\right)}{\partial x} + M_y\left(\sum_{i=1}^{n} H_y^i\right)\frac{\partial\left(\sum_{i=1}^{n} H_z^i\right)}{\partial y} + M_z\left(\sum_{i=1}^{n} H_z^i\right)\frac{\partial\left(\sum_{i=1}^{n} H_z^i\right)}{\partial z} \end{pmatrix}_{(x,y,z)} \tag{16}$$

3 Results and discussion

3.1 Simulation of the 3D magnetic fields

Previously, a case of magnetophoresis in 2D was studied in Anne-Laure Gaussner et al.'s paper (2009) with magnets arranged in repulsive and attractive configurations. In their work, 2D field distribution was simulated using finite element method (FEM). We choose to compare results from our 3D and analytical model to theirs using same simulation parameters except the length of the magnet in z-direction is set to be very large ($w/l = 10{,}000$) so that our force distributions using exactly the same parameters in Anne-Laure Gassner et al's. paper (2009). Our analytical results agree extremely well to their FEM results. We will use this fast and precise analytical magnetic field model in studying particles' trajectories in magnetic fluids.

3.2 Simulation of a permanent magnet-based separation device

Using permanent magnets to focus and separate non-magnetic particles and cells in ferrofluids has been experimentally studied recently (Zhu et al. 2010, 2011b; Liang

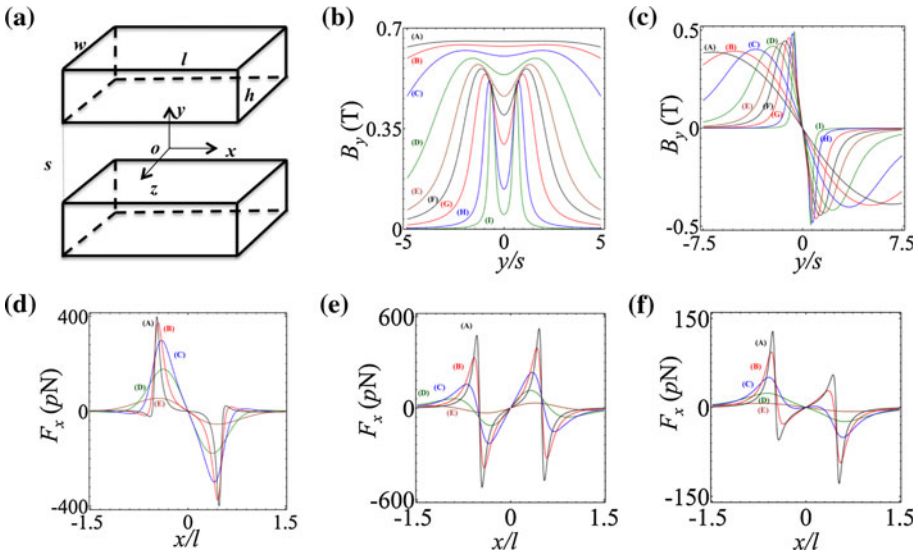

Fig. 3 **a** A pair of rectangular permanent magnets with their magnetization in y-direction. The dimensions of the magnets are labeled as l, h, w while $w/l = 10{,}000$ and the distance s between them is fixed at 200 μm. **b** Relationship between the y component of magnetic flux density B_y along y-direction at $x = 0$ and the ratio l/s = *(A)* 10, *(B)* 7.5, *(C)* 5, (D) 3, *(E)* 2, *(F)* 1.5, *(G)* 1, *(H)* 0.5, *(I)* 0.25 when the magnets are placed in an attractive manner. **c** Relationship between the y component of magnetic flux density B_y along y-direction at $x = 0$ and the ratio l/s = *(A)* 10, *(B)* 7.5, *(C)* 5, *(D)* 3, *(E)* 2, *(F)* 1.5, *(G)* 1, *(H)* 0.5, *(I)* 0.25 when the magnets are placed in a repulsive manner. **d** Relationship between the x component of magnetic force F_x along x-direction at $y = 0$ and the ratio l/s = *(A)* 10, *(B)* 5, *(C)* 2, *(D)* 1, *(E)* 0.5 when the magnets are placed in an attractive manner. **e** Relationship between the x component of magnetic force F_x along x-direction at $y = 0$ and the ratio l/s = *(A)* 10, *(B)* 5, *(C)* 2, *(D)* 1, *(E)* 0.5 when the magnets are placed in a repulsive manner. **d** Relationship between the x component of magnetic force F_x along x-direction at $y = 0$ and the ratio l/s = *(A)* 10, *(B)* 5, *(C)* 2, *(D)* 1, *(E)* 0.5 when there is only one magnet. All calculations are done on a particle with 1 μm diameter and initial susceptibility of 1. These parameters are chosen to be the same in Anne-Laure Gassner et al's paper (2009)

et al. 2011). In these studies, non-magnetic objects were mixed with ferrofluid and introduced into a ferrofluid-filled microchannel. These objects experienced magnetic buoyancy force on them and were deflected out of their flow paths toward the weaker magnetic field direction. Object of larger size experienced larger magnetic force. This size-based deflection was used for focusing and separation of particles and cells. Here, we study a single permanent magnet-based ferrofluidic device and investigate the dependence of particle deflection on both fluidic and geometric parameters. The system considered in our model consists of a microfluidic channel and a permanent magnet with dimensions illustrated in Fig. 4.

We consider a 3D model, in which a rectangular magnet of length l_m, height h_m and width w_m is symmetrically aligned to a rectangular channel of length l_c, height h_c and width w_c as shown in Fig. 4. Symbols Δy and Δz are relative distances between the magnet and the channel in y and z-directions, respectively. Ferrofluid flow is introduced into the microchannel in positive x-direction, while the particles are released at left bottom point with the coordinate $(-l_c/2,-h_c/2, 0)$ in Fig. 4a. When there is no magnetic field, the particles follow their laminar paths and exit the channel at the right-bottom point of coordinate $(l_c/2,-h_c/2, 0)$ in Fig. 4a. When a rectangular magnet is placed at the center of the channel length with its magnetic pole perpendicular to the channel wall, its field magnetizes the ferrofluid within the channel and subsequently deflects the particle trajectories toward positive y-direction, as shown in Fig. 4a, b. We use parameters listed in Table 1 in our simulation. These parameters are chosen to mimic a typical microfluidic separation device using ferrofluids.

Figure 5 shows the simulated strength and directions of magnetic fields and magnetic buoyancy forces on a 4-μm-diameter non-magnetic particle in our system, as well as the 3D trajectories of non-magnetic particles with diameter ranging from 2 to 8 μm.

The surface plot in Fig. 5a shows magnitudes of magnetic fields of x–y plane at $z = 0$. Magnetic fields decay quickly from the surface of magnet and form a gradient that results in magnetic buoyancy force on particles in both x- and y-directions, as indicated in Fig. 5b. Consequently, non-magnetic particles experiencing such force after entering the channel decelerate in x-direction and accelerate in y-direction. Force computed on a spherical microparticle of 4 μm diameter, with its total volume close to 30 μm^3, is on the order of 10 pN. Particle mixtures are deflected differently by the magnetic buoyancy force toward the end of channel, as shown in Fig. 5c with simulated trajectories. From the trajectories of particles with different diameters in Fig. 5c, larger particles experience larger magnetic buoyancy forces, which result in larger deflection in y-direction. Figure 5d–f illustrates distribution of magnetic fields and forces on y–z plane at $x = 0$, as well as the projection of particles' trajectories, while Fig. 5g–i depicts the cases of x–z plane at $y = 0$. The total deflection of a particle in this configuration is a product of their y-direction migration velocity and their residual time in the channel. We notice that particles are quickly pushed down in z-direction toward the bottom surface after they enter the channel. This significantly affects their flow velocities in x-direction as the ferrofluid flow profile has a parabolic shape across the channel depth. The closer the particles to the channel surface, the slower their flow velocities are. The residual time of the particles will increase as a result, which will in turn affect their overall deflection. On the other hand, as the particles approach the channel surface, they experience an increased fluid viscosity because of the "wall effect." This will affect their migration velocity in y-direction and their overall deflection, too. Therefore, locations of particles in z-direction (channel depth) are critical information that should be available to the investigators and can only be simulated through a true 3D model.

3.3 Effects of physical properties on particle deflection

Both the magnetic buoyancy force and hydrodynamic drag force are greatly impacted by physical properties of ferrofluids and permanent magnets. Studying the effect of these properties on particle deflection is critical in optimizing magnetic fluid-based microfluidic devices. We focus our discussion on four important physical properties in our system including ferrofluid flow rate Q, magnetization of permanent magnet M_s, volume fraction of magnetic materials in ferrofluids ϕ and average diameter of magnetic nanoparticles d.

Figure 6 summarizes the dependence of particle deflection $D_{\text{deflection}}$, particle residual time in the channel t and average particle velocity in y-direction U_D on the above-mentioned four properties. All other parameters in this simulation remain the same as they are listed in Table 1. Figure 6a shows the particle deflection ($D_{\text{deflection}}$, Blue square), residual time (t, green circle) and the particle velocity (U_D, red diamond) at different flow rates Q of the ferrofluid. When the flow rate increases, the residual time t of the particles decreases, resulting in a smaller deflection $D_{\text{deflection}}$ for the particle. The average particle velocity in y-direction U_D increases in our simulation. Generally speaking, U_D is determined by balancing magnetic and hydrodynamic viscous forces. In a system where only flow rates are changing, U_D should remain the same. This is true only in 2D cases. In our 3D model though, we consider an additional dimension of z-direction, which makes particles' trajectories more complicated than the 2D case. At a smaller flow rate, particles are pushed down toward the

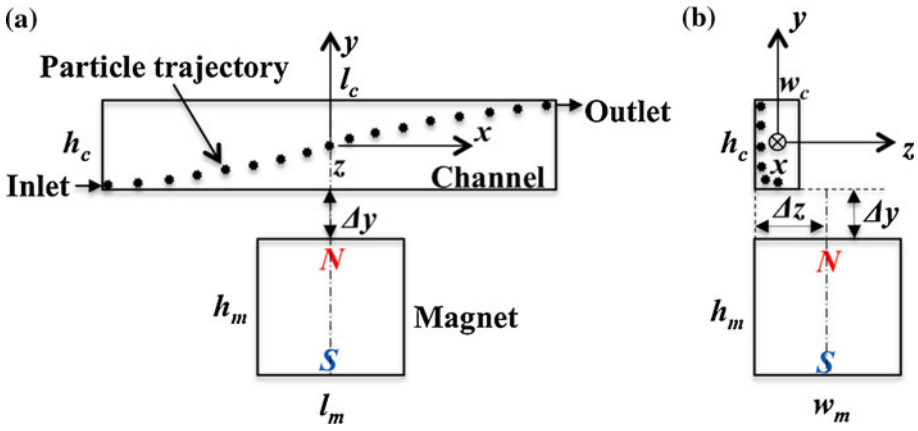

Fig. 4 **a** Schematic representation of the microchannel with a permanent magnet in x–y plane. **b** Cross section of the device. All the dimensions of channel (l_c, h_c, w_c) and magnet (l_m, h_m, w_m) as well as their relative positions (Δy, Δz) are labeled

Table 1 Physical and geometrical parameters used in the simulation

Symbol	Name	Initial value
Constants		
κ_B	Boltzmann constant	1.38×10^{-23} J/K
μ_0	Permeability of free space	$4\pi \times 10^{-7}$ H/m
ϕ_c	Critical volume fraction	0.74
Environmental conditions		
T	Temperature	298 K
Non-magnetic particles		
D_p	Diameter	4 μm
Ferrofluid:		
d	Diameter of the nanoparticles	10 nm
ε	Thickness of the coating layer	2 nm
M_d	Bulk magnetization of Fe_3O_4	4.46×10^5 A/m
ϕ	Volume fraction of magnetic nanoparticles	0.01
η_c	Dynamic viscosity of carrier liquid (water)	1 mPa.s
Q	Flow rate of ferrofluid	6 μL/min
Permanent magnet		
M_s	Magnetization of magnet	3.18×10^5 A/m
l_m	Length of magnet	5 mm
h_m	Height of magnet	8 mm
w_m	Width of magnet	3 mm
Microchannel		
l_c	Length of channel	20 mm
h_c	Height of channel	3 mm
w_c	Width of channel	0.05 mm
Relative distance		
Δy	Between channel and magnet in y-direction	1 mm
Δz	Between channel and magnet in z-direction	1.5 mm

channel surface earlier than at a higher flow rate. Moving along channel surfaces increases the fluid viscosity the particle sees, which in turn decreases its migration velocity U_D in y-direction. This effect appears to be vital in determining overall particle trajectory and can be fully studied in our 3D model. Figure 6b shows the effect of magnetization M_s of the magnet on particle deflection. Strength of magnetic field $\vec{H}$ of a permanent magnet is proportional its remanent magnetization M_s. Larger magnetic fields naturally lead to larger magnetic buoyance forces on particles, rendering a increase of U_D and $D_{\text{deflection}}$. Figure 6c, d shows the dependence of particle deflection on physical properties of ferrofluids including volume fraction ϕ and average diameter d of magnetic nanoparticles in the fluid. We discuss these two properties together because of their effects on particle deflection are alike. First, both of their increases will give rise to the magnetization of ferrofluids according to Eq. (6), which increases the magnitude of magnetic buoyancy force. Second, their increases will also raise the viscosity of ferrofluids according to Eq. (12), and eventually increase the magnitude of hydrodynamic drag force, which is always against the magnetic buoyancy force as it tries to minimize the relative motion between the particles and the fluid. Considering the practical range of ϕ and d for typical water-based ferrofluids used in microfluidics, and other realistic experimental conditions, enhancement of the magnetic buoyancy force by increasing these two parameters appears to be larger than that of hydrodynamic drag force, as evidenced by Figs. 6c, d where $D_{\text{deflection}}$ and U_D both increase for larger values of ϕ and d.

3.4 Effects of geometrical parameters on particle deflection

In addition to physical properties, geometrical parameters such as dimensions of the permanent magnet and relative positions between the magnet and the channel have significant effects on particle deflection. In this section, we will discuss the effects of these parameters. In order to represent dimensions and relative positions of the magnet,

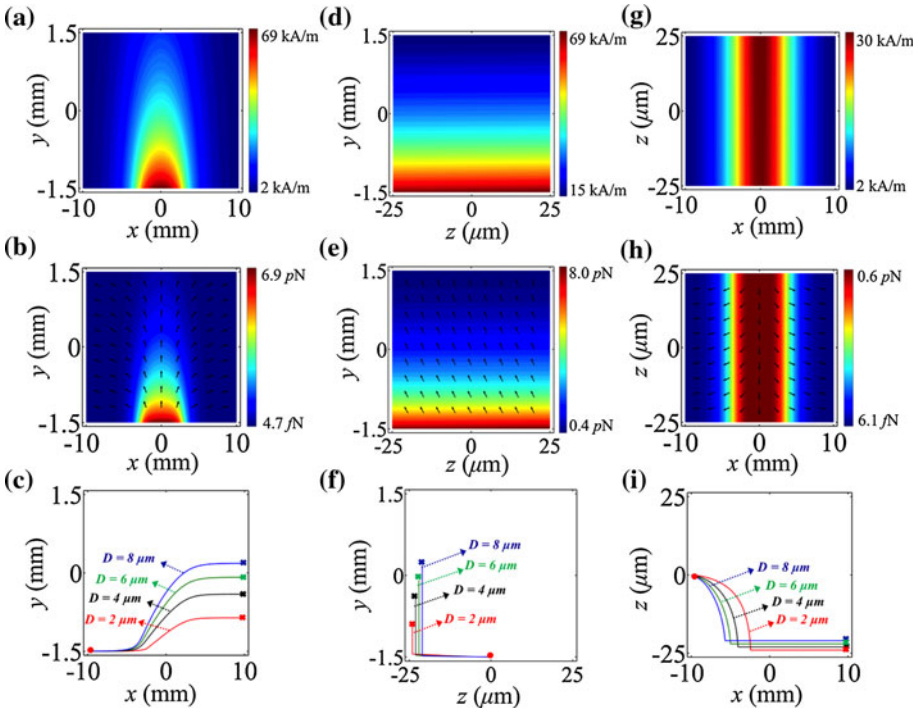

Fig. 5 Analytical three-dimensional simulation of magnetic field and force distributions in the microchannel, and trajectories of particles with different sizes (2–8 μm). Other simulation parameters are listed in Table 1. **a**–**c** *x*–*y* plane ($z = 0$), **d**–**f** *y*–*z* plane ($x = 0$), **g**–**i** *x*–*z* plane ($y = 0$) of magnetic field strength (*surface plot*) (**a**, **d**, **g**), magnetic force (*surface plot*: force magnitude; *arrow plot*: force direction; both are calculated on a 4-μm-diameter non-magnetic particle) (**b**, **e**, **h**), and projection of particles' trajectories (**c**, **f**, **i**). *Dots* indicate starting points, while *crosses* indicate ending points of particles' trajectories

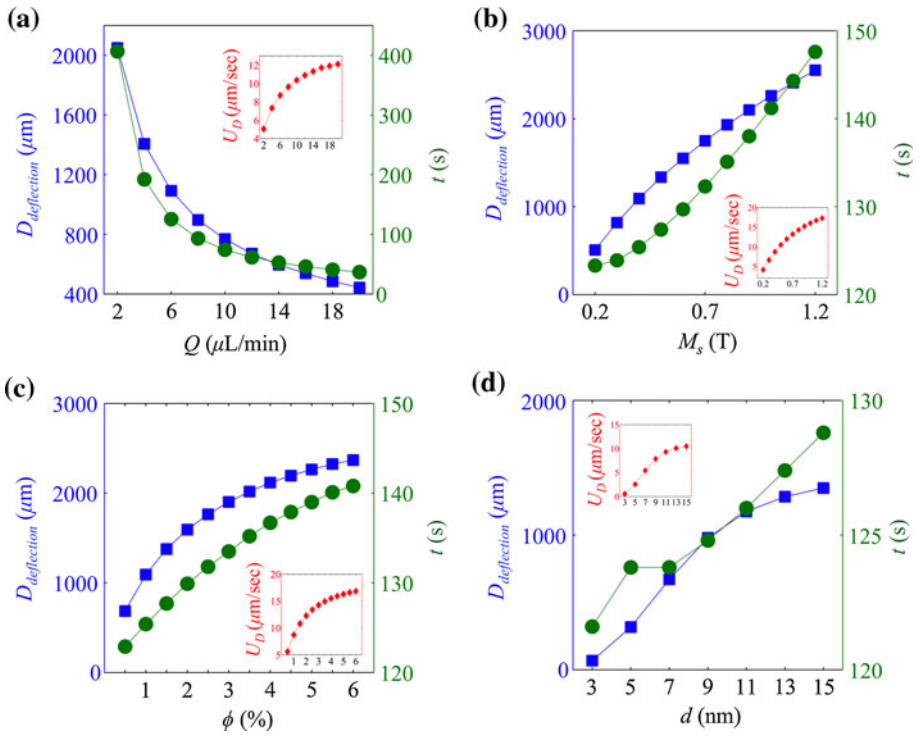

Fig. 6 Simulation results of particle deflection ($D_{deflection}$, *blue square*), residual time (*t*, *green circle*) and average particle migration velocity in *y*-direction (U_D, *red diamond*) with respect to different **a** flow rate *Q*; **b** residual magnetization M_s; **c** volume fraction ϕ and **d** size of magnetic nanoparticles *d* in ferrofluids (color figure online)

we keep its width w_m as a constant while changing its length l_m and height h_m. The magnet and channel are equally divided by *y*-axis in *x*–*y* plane as shown in Fig. 4a. We vary the relative position between the magnet and the channel in *y*–*z* plane, which is labeled by Δy and Δz, as shown in Fig. 4b. All of the above variables (l_m, h_m, Δy, Δz) are normalized through dividing them by the width of magnet w_m. As a result, we obtain four dimensionless parameters (α, β, γ, δ) in Eq. (17).

$$\alpha = \frac{l_m}{w_m}, \beta = \frac{h_m}{w_m}, \gamma = \frac{\Delta y}{w_m}, \delta = \frac{\Delta z}{w_m}, \tag{17}$$

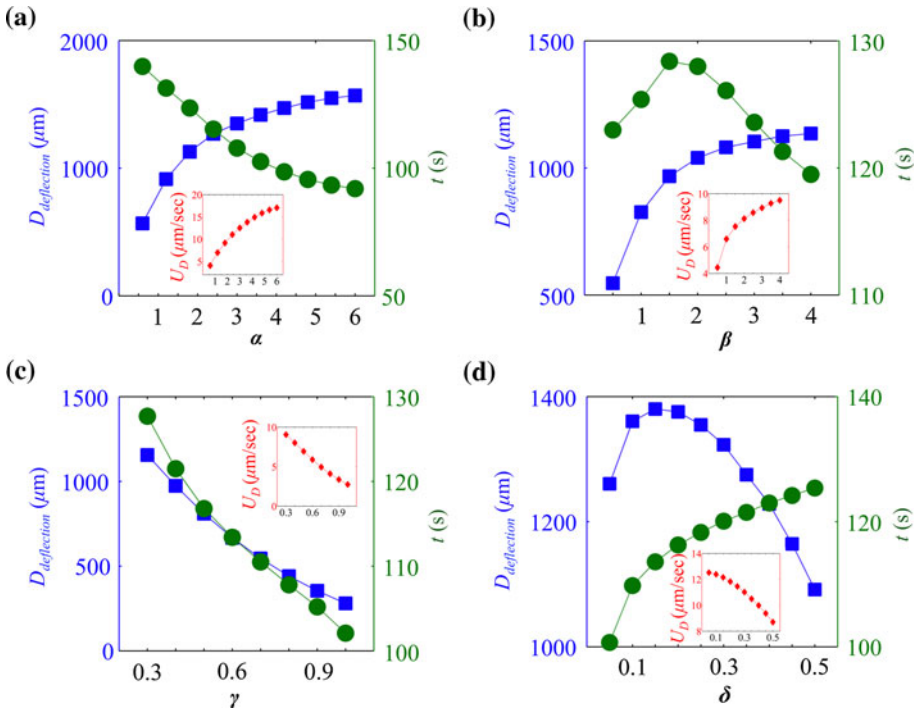

Fig. 7 Simulation results of particle deflection ($D_{\text{deflection}}$, *blue square*), residual time (t, *green circle*) and average particle migration velocity in y-direction (U_D, *red diamond*) with respect to different values of aspect ratios **a** $\alpha = l_m/w_m$; **b** $\beta = h_m/w_m$; **c** $\gamma = \Delta y/w_m$ and **d** $\delta = \Delta z/w_m$ (color figure online)

As it is discussed before, the total deflection of a particle is a product of their y-direction migration velocity U_D and their residual time t. U_D is proportional to the magnitude of magnetic buoyance force and inversely proportional to the fluid viscosity. t on the other hand depends on the location of particle's laminar flow layer and subsequently the particle's z location. We expect the magnetic field, magnetic buoyance force, fluid viscosity, as well as the particle's z location will change as we vary any of the four dimensionless parameters above. These changes in turn will affect U_D and t in a profound way resulting in overall particle deflection $D_{\text{deflection}}$ change. The effects from these parameters on particle velocity and residual time are highly coupled. It is therefore difficult and counter-intuitive to try to offer straightforward explanations for some of these effects. Instead we will simply summarize our simulation results on these parameters as follows. Figure 7 shows the dependence of $D_{\text{deflection}}$, U_D and t on the four dimensionless parameters. All other parameters in this simulation remain the same as they are listed in Table 1. Figure 7a shows the dependence of particle deflection ($D_{\text{deflection}}$, blue square), residual time (t, green circle) and the average particle migration velocity in y-direction (U_D, red diamond) on α. $D_{\text{deflection}}$ has a monotonic increase when α increases, because of the reduced residual time t and increased U_D. Figure 7b shows the effect of β on particle deflection, while Fig. 7c shows the effect of distance between the magnet and channel. As the magnet is getting further away from the channel, both magnetic field and force decrease, rendering smaller overall deflection. Finally, Fig. 7d shows the effect of δ, where it appears to have a critical value of $\delta = 0.15$ leading maximum particle deflection.

4 Conclusion

In conclusion, we develop a 3D analytical model to study microfluidic motions of non-magnetic particles in magnetic fluids. This model can predict magnetic fields and force, hydrodynamic drag force, fluid flow profiles, particle deflection, particle residual time and particle velocity in a 3D microfluidic system coupled with permanent magnets. The model can be used to study and optimize magnetic fluid-based devices on their physical properties and geometrical parameters. The simplicity and the versatility of this 3D model make it attractive for quick optimizations and design of devices. We envision it will help design more efficient microfluidic manipulation systems design based on magnetic fluids.

Acknowledgments This work is supported by the National Science Foundation and the Office of Vice President for Research at the University of Georgia.

References

Adams AA, Okagbare PI, Feng J, Hupert ML, Patterson D, Gottert J, McCarley RL, Nikitopoulos D, Murphy MC, Soper SA (2008) Highly efficient circulating tumor cell isolation from whole

blood and label-free enumeration using polymer-based microfluidics with an integrated conductivity sensor. J Am Chem Soc 130(27):8633–8641. doi:10.1021/Ja8015022

Beyor N, Seo TS, Liu P, Mathies RA (2008) Immunomagnetic bead-based cell concentration microdevice for dilute pathogen detection. Biomed Microdevices 10(6):909–917. doi:10.1007/S10544-008-9206-3

Bonner WA, Sweet RG, Hulett HR, Herzenbe La (1972) Fluorescence activated cell sorting. Rev Sci Instrum 43(3):404

Brody JP, Yager P, Goldstein RE, Austin RH (1996) Biotechnology at low Reynolds numbers. Biophys J 71(6):3430–3441

Davis JA, Inglis DW, Morton KJ, Lawrence DA, Huang LR, Chou SY, Sturm JC, Austin RH (2006) Deterministic hydrodynamics: taking blood apart. Proc Natl Acad Sci USA 103(40): 14779–14784. doi:10.1073/Pnas.0605967103

Dharmasiri U, Witek MA, Adams AA, Osiri JK, Hupert ML, Bianchi TS, Roelke DL, Soper SA (2010) Enrichment and detection of *Escherichia coli* O157:H7 from water samples using an antibody modified microfluidic chip. Anal Chem 82(7):2844–2849. doi:10.1021/Ac100323k

Furlani EP (2001) Permanent magnet and electromechanical devices. Academic Press, New York

Furlani EP (2006) Analysis of particle transport in a magnetophoretic microsystem. J Appl Phys 99(2):024912

Furlani EP (2007) Magnetophoretic separation of blood cells at the microscale. J Phys D Appl Phys 40(5):1313

Furlani EP, Sahoo Y (2006) Analytical model for the magnetic field and force in a magnetophoretic microsystem. J Phys D Appl Phys 39(9):1724

Ganatos P, Weinbaum S, Pfeffer R (1980) A strong interaction theory for the creeping motion of a sphere between plane parallel boundaries. Part 1. Perpendicular motion. J Fluid Mech 99(04):739–753. doi:10.1017/S0022112080000870

Gassner A-L, Abonnenc M, Chen H-X, Morandini J, Josserand J, Rossier JS, Busnel J-M, Girault HH (2009) Magnetic forces produced by rectangular permanent magnets in static microsystems. Lab Chip 9(16):2356–2363

Gijs MAM, Lacharme F, Lehmann U (2010) Microfluidic applications of magnetic particles for biological analysis and catalysis. Chem Rev 110(3):1518–1563. doi:10.1021/Cr9001929

Gossett DR, Weaver WM, Mach AJ, Hur SC, Tse HTK, Lee W, Amini H, Di Carlo D (2010) Label-free cell separation and sorting in microfluidic systems. Anal Bioanal Chem 397(8):3249–3267. doi:10.1007/S00216-010-3721-9

He L, Hu Y, Kim H, Ge J, Kwon S, Yin Y (2010) Magnetic assembly of nonmagnetic particles into photonic crystal structures. Nano Lett 10(11):4708–4714. doi:10.1021/nl103008v

Hoshino K, Huang YY, Lane N, Huebschman M, Uhr JW, Frenkel EP, Zhang XJ (2011) Microchip-based immunomagnetic detection of circulating tumor cells. Lab Chip 11(20):3449–3457. doi:10.1039/C1lc20270g

Huang LR, Cox EC, Austin RH, Sturm JC (2004) Continuous particle separation through deterministic lateral displacement. Science 304(5673):987–990

Huang P, Guasto JS, Breuer KS (2006) Direct measurement of slip velocities using three-dimensional total internal reflection velocimetry. J Fluid Mech 566:447–464. doi:10.1017/S0022112006002229

Ichikawa N, Hosokawa K, Maeda R (2004) Interface motion of capillary-driven flow in rectangular microchannel. J Colloid Interface Sci 280(1):155–164. doi:10.1016/j.jcis.2004.07.017

Kose AR, Fischer B, Mao L, Koser H (2009) Label-free cellular manipulation and sorting via biocompatible ferrofluids. Proc Natl Acad Sci. doi:10.1073/pnas.0912138106

Krishnan GP, David T, Leighton J (1995) Inertial lift on a moving sphere in contact with a plane wall in a shear flow. Phys Fluids 7(11):2538–2545

Laurell T, Petersson F, Nilsson A (2007) Chip integrated strategies for acoustic separation and manipulation of cells and particles. Chem Soc Rev 36(3):492–506. doi:10.1039/B601326k

Lee H, Purdon AM, Chu V, Westervelt RM (2004) Controlled assembly of magnetic nanoparticles from magnetotactic bacteria using microelectromagnets arrays. Nano Lett 4(5):995–998. doi:10.1021/Nl049562x

Lenshof A, Laurell T (2010) Continuous separation of cells and particles in microfluidic systems. Chem Soc Rev 39(3):1203–1217. doi:10.1039/B915999c

Liang L, Zhu J, Xuan X (2011) Three-dimensional diamagnetic particle deflection in ferrofluid microchannel flows. Biomicrofluidics 5(3):034110

Liu RH, Yang JN, Lenigk R, Bonanno J, Grodzinski P (2004) Self-contained, fully integrated biochip for sample preparation, polymerase chain reaction amplification, and DNA microarray detection. Anal Chem 76(7):1824–1831. doi:10.1021/Ac0353029

Liu CX, Stakenborg T, Peeters S, Lagae L (2009), Cell manipulation with magnetic particles toward microfluidic cytometry. J Appl Phys 105(10):102014-1–102014-11

Mao X, Huang TJ (2012a) Exploiting mechanical biomarkers in microfluidics. Lab Chip 12(20):4006–4009. doi:10.1039/c2lc90100e

Mao X, Huang TJ (2012b) Microfluidic diagnostics for the developing world. Lab Chip 12(8):1412–1416. doi:10.1039/c2lc90022j

McFaul SM, Lin BK, Ma H (2012) Cell separation based on size and deformability using microfluidic funnel ratchets. Lab Chip 12(13):2369–2376. doi:10.1039/c2lc21045b

Nagrath S, Sequist LV, Maheswaran S, Bell DW, Irimia D, Ulkus L, Smith MR, Kwak EL, Digumarthy S, Muzikansky A, Ryan P, Balis UJ, Tompkins RG, Haber DA, Toner M (2007) Isolation of rare circulating tumour cells in cancer patients by microchip technology. Nature 450(7173):1235–1239. doi:10.1038/Nature06385

Odenbach S (2002) Magnetoviscous effects in ferrofluids. Springer, New York

Pamme N (2006) Magnetism and microfluidics. Lab Chip 6(1):24–38. doi:10.1039/B513005k

Pamme N (2007) Continuous flow separations in microfluidic devices. Lab Chip 7(12):1644–1659. doi:10.1039/B712784g

Pethig R (2010) Review article—dielectrophoresis: status of the theory, technology, and applications. Biomicrofluidics 4(2): 022811

Robert D, Pamme N, Conjeaud H, Gazeau F, Iles A, Wilhelm C (2011) Cell sorting by endocytotic capacity in a microfluidic magnetophoresis device. Lab Chip 11(11):1902–1910. doi:10.1039/c0lc00656d

Rosensweig RE (1985) Ferrohydrodynamics. Cambridge University Press, Cambridge

Shen F, Hwang H, Hahn YK, Park J-K (2012) Label-free cell separation using a tunable magnetophoretic repulsion force. Anal Chem 84(7):3075–3081. doi:10.1021/ac201505j

Shi JJ, Huang H, Stratton Z, Huang YP, Huang TJ (2009) Continuous particle separation in a microfluidic channel via standing surface acoustic waves (SSAW). Lab Chip 9(23):3354–3359. doi:10.1039/B915113c

Staben ME, Zinchenko AZ, Davis RH (2003) Motion of a particle between two parallel plane walls in low-Reynolds-number Poiseuille flow. Phys Fluids 15(6):1711–1733

Tarn MD, Peyman SA, Pamme N (2013) Simultaneous trapping of magnetic and diamagnetic particle plugs for separations and bioassays. RSC Advances 3(20):7209–7214. doi:10.1039/c3ra40237a

Toner M, Irimia D (2005) Blood-on-a-chip. Annu Rev Biomed Eng 7:77–103. doi:10.1146/Annurev.Bioeng.7.011205.135108

Tsutsui H, Ho CM (2009) Cell separation by non-inertial force fields in microfluidic systems. Mech Res Commun 36(1):92–103. doi:10.1016/J.Mechrescom.2008.08.006

Vojtíšek M, Tarn M, Hirota N, Pamme N (2012) Microfluidic devices in superconducting magnets: on-chip free-flow diamagnetophoresis of polymer particles and bubbles. Microfluid Nanofluid 13(4):625–635. doi:10.1007/s10404-012-0979-6

Voldman J (2006) Electrical forces for microscale cell manipulation. Annu Rev Biomed Eng 8:425–454. doi:10.1146/Annurev.Bioeng.8.061505.095739

Wang FC, Zhao YP (2011) Slip boundary conditions based on molecular kinetic theory: the critical shear stress and the energy dissipation at the liquid-solid interface. Soft Matter 7(18):8628–8634. doi:10.1039/C1sm05543g

Wang ZC, Zhe JA (2011) Recent advances in particle and droplet manipulation for lab-on-a-chip devices based on surface acoustic waves. Lab Chip 11(7):1280–1285. doi:10.1039/C0lc00527d

Winkleman A, Gudiksen KL, Ryan D, Whitesides GM, Greenfield D, Prentiss M (2004) A magnetic trap for living cells suspended in a paramagnetic buffer. Appl Phys Lett 85(12):2411–2413

Yamada M, Nakashima M, Seki M (2004) Pinched flow fractionation: continuous size separation of particles utilizing a laminar flow profile in a pinched microchannel. Anal Chem 76(18):5465–5471. doi:10.1021/Ac049863r

Yellen BB, Hovorka O, Friedman G (2005) Arranging matter by magnetic nanoparticle assemblers. Proc Natl Acad Sci USA 102(25):8860–8864

Yung CW, Fiering J, Mueller AJ, Ingber DE (2009) Micromagnetic-microfluidic blood cleansing device. Lab Chip 9(9):1171–1177. doi:10.1039/B816986a

Zborowski M, Ostera GR, Moore LR, Milliron S, Chalmers JJ, Schechter AN (2003) Red blood cell magnetophoresis. Biophys J 84(4):2638–2645. doi:10.1016/S0006-3495(03)75069-3

Zeng J, Chen C, Vedantam P, Brown V, Tzeng T-RJ, Xuan X (2012) Three-dimensional magnetic focusing of particles and cells in ferrofluid flow through a straight microchannel. J Micromech Microeng 22(10):105018

Zhang K, Liang Q, Ai X, Hu P, Wang Y, Luo G (2011) On-demand microfluidic droplet manipulation using hydrophobic ferrofluid as a continuous-phase. Lab Chip 11(7):1271–1275. doi:10.1039/c0lc00484g

Zhu TT, Marrero F, Mao LD (2010) Continuous separation of non-magnetic particles inside ferrofluids. Microfluid Nanofluid 9(4–5):1003–1009. doi:10.1007/S10404-010-0616-1

Zhu T, Cheng R, Mao L (2011a) Focusing microparticles in a microfluidic channel with ferrofluids. Microfluid Nanofluid 11(6):695–701. doi:10.1007/s10404-011-0835-0

Zhu T, Lichlyter D, Haidekker M, Mao L (2011b) Analytical model of microfluidic transport of non-magnetic particles in ferrofluids under the influence of a permanent magnet. Microfluid Nanofluid 10(6):1233–1245. doi:10.1007/s10404-010-0754-5

Zhu TT, Cheng R, Lee SA, Rajaraman E, Eiteman MA, Querec TD, Unger ER, Mao LD (2012) Continuous-flow ferrohydrodynamic sorting of particles and cells in microfluidic devices. Microfluid Nanofluid 13(4):645–654. doi:10.1007/S10404-012-1004-9